Relative dispersion observations and trajectory modeling in the Santa Barbara Channel

J. Carter Ohlmann,[1] Joe H. LaCasce,[2] Libe Washburn,[3] Arthur J. Mariano,[4] and Brian Emery[3]

Received 6 December 2011; revised 19 March 2012; accepted 14 April 2012; published 26 May 2012.

[1] Relative dispersion statistics and related Lagrangian parameters, not well observed in coastal regions, are obtained from in situ surface drifter observations and presented in the context of Lagrangian stochastic models. Clusters of GPS tracked surface drifters, with initial horizontal spacing of 5–10 m, were repetitively deployed in the Santa Barbara Channel from July 2004 to June 2005. The drifters sampled their position every 10 min for 1–2 days. Mean square pair separation distance, or relative dispersion, increases approximately exponentially in time during the first ~5 h of sampling (e-folding time of 0.9 h). Thereafter, the dispersion increase is approximately quadratic in time. Large error bars on the observed mean dispersion, and higher-order Lagrangian statistics that are not clearly supportive of the aforementioned dispersion curves, indicate uncertainty. The mean square relative (separation) velocity shows near-linear growth with pair separation distance, extending from 0.3 to 85 $cm^2\ s^{-2}$ over length scales from ~8 m to 2.2 km. The observed length scale dependency in square relative velocity is investigated in a Lagrangian stochastic model (LSM) for a cloud of particles. Modeled dispersion agrees with observations only when the velocity scale for the sub-grid scale random normal deviate in the LSM (typically a constant) is length scale dependent, and takes into consideration the observed scaling. Occasional large (>25 $cm\ s^{-1}$) discrepancies in grid-scale velocities between drifters and HF radar cause general disagreement in distributions of ending positions of LSM trajectories when compared with Lagrangian observations.

Citation: Ohlmann, J. C., J. H. LaCasce, L. Washburn, A. J. Mariano, and B. Emery (2012), Relative dispersion observations and trajectory modeling in the Santa Barbara Channel, *J. Geophys. Res.*, *117*, C05040, doi:10.1029/2011JC007810.

1. Introduction

[2] Knowledge of transport pathways, or particle trajectories, in the coastal ocean is necessary for addressing a wide range of applied oceanographic problems that include connectivity among marine protected areas (MPAs), determining the origin or fate of contaminated waters, and for search-and-rescue activities. For example, trajectories derived from numerical simulations [*Mitarai et al.*, 2009] were considered during the process of determining an optimum Southern California MPA network. Search-and-rescue operations typically rely on surface current trajectories determined from a combination of both real-time and historical observations, numerical model simulations, and Lagrangian stochastic models (LSMs).

[3] Coastal circulation observations and modeling efforts have recently expanded in response to health, safety, and economic concerns. High frequency (HF) radar observations that provide time and space averaged maps of surface currents from the coast to roughly 150 km offshore are presently available for many coastal regions [*Kim et al.*, 2011]. Spatial resolution of HF radar surface currents ranges from ~1 to 10 km. LSMs can be used with Eulerian HF radar surface current maps to determine trajectory information in the coastal ocean [e.g., *Spaulding et al.*, 2006]. However, little is known about turbulent processes that act on scales smaller than resolved with HF radar, scales of a few kilometers and less.

[4] Dispersion in the coastal ocean can be considered in both Eulerian and Lagrangian reference frames. In the Eulerian view, the temporal evolution of the spatial distribution of the statistical moments (mean, variance), or probability density function, of a concentration field is analyzed. The time (t) evolution of the concentration field (C) is generally modeled as an advection-diffusion process

$$\frac{\partial C}{\partial t} = -\boldsymbol{U} \cdot \nabla C + \nabla \cdot (\mathbf{K} \cdot \nabla C), \qquad (1)$$

[1]Institute for Computational Earth System Science, University of California, Santa Barbara, California, USA.
[2]Department of Geosciences, University of Oslo, Oslo, Norway.
[3]Marine Science Institute, University of California, Santa Barbara, California, USA.
[4]Division of Meteorology and Physical Oceanography, Rosenstiel School of Marine and Atmospheric Science, University of Miami, Miami, Florida, USA.

Corresponding author: J. C. Ohlmann, Institute for Computational Earth System Science, University of California, Santa Barbara, CA 93106, USA. (carter@eri.ucsb.edu)

0148-0227/12/2011JC007810

where $\boldsymbol{U}$ is the large-scale velocity vector, and $\mathbf{K}$ is a diffusivity coefficient tensor typically used to parameterize the turbulent processes [*Taylor*, 1922]. Significant inhomogeneities in $\mathbf{K}$ can exist in coastal regions, and arise from a number of factors including variable bathymetry and coastline shape [*Swenson and Niiler*, 1996]. Furthermore, the formulation assumes scale separation that is not typically valid [*Davis*, 1987]. The classic advection-diffusion model may not be optimal for applications in coastal circulation.

[5] Particle transport in the Lagrangian view is due to advection by $\boldsymbol{U}$, and to a sub-grid scale velocity associated with processes not contained in $\boldsymbol{U}$. The basic assumption of the auto-regressive order-one LSM is that sub-grid scale variability is not white noise but contains a colored component due to autocorrelation in time. Auto-regressive order-one LSMs have been used to model the unresolved velocity variability for computation of particle trajectories in the open ocean [*Griffa et al.*, 1995; *Veneziani et al.*, 2004], coastal ocean [*Ullman et al.*, 2006] and the atmospheric boundary layer [*Wilson and Sawford*, 1996].

[6] Particle pairs in turbulent flows separate, on average, in time; and the rate of separation generally depends on pair separation distance itself [e.g., *Richardson*, 1926; *Batchelor and Townsend*, 1953; *Bennett*, 1984; *Babiano et al.*, 1990; *LaCasce*, 2008]. In the order-one LSM, particles move independently of one another. Thus, in most situations, the LSM does not simulate the *relative* motion of particle pairs (stochastic models for particle-pair dispersion are described by *Sawford* [2001], and references therein). However, since the spatial variance of a cloud of particles is formally related to the mean square separation velocity of particle pairs in the cloud [e.g., *LaCasce*, 2008], LSMs can be used to simulate cloud dispersion.

[7] In a number of recent studies, single-particle LSMs are used for coastal circulation applications. For instance, the LSM described by *Paris et al.* [2007] increases the accuracy of larval dispersal distance estimates. *Ullman et al.* [2006] show an improvement in predicted search area with trajectories determined from a LSM. These studies indicate successful application of LSMs despite uncertainty in model parameters assumed. The studies obtain sub-grid scale velocity quantities from Eulerian model output on a 2×2 km grid, and instantaneous differences between drifter and HF radar velocities. Two-particle stochastic models have not yet been employed in such applications. Thus, it is unknown whether enhanced representation of turbulent pair separation in such models can improve agreement with dispersion observations.

[8] This study presents relative dispersion quantities in the coastal ocean observed over spatial scales from roughly 5 m to 2 km. Measurements at these scales are scarce. The observations can help improve sub-grid scale parameterizations in ocean models. The data are then used to investigate whether enhanced representation of turbulent pair separation in a LSM can improve agreement with dispersion observations. Both the LSM form and empirical model parameters are considered. Drifting buoy observations collected in the northern Santa Barbara Channel (SBC) are the basis of the study. The instrumentation, deployment scheme, and data processing methods are described in section 2. Also presented in section 2 is the LSM used to model relative dispersion, and associated model parameters. Results that include drifter observations; relative dispersion values; empirically determined LSM parameters; and the sensitivity of modeled dispersion to various forms of the LSM, its parameters, and their scalings are presented in section 3. These results are discussed in section 4, and conclusions are given in section 5.

2. Methods

2.1. Drifter Data

[9] Position data are recorded with Microstar drifters, manufactured by Pacific Gyre Corporation (Oceanside, CA) specifically for use in coastal regions [*Ohlmann et al.*, 2005]. Drifters record their position every 10 min using the Global Positioning System (GPS), and transmit their data in near real-time using the Iridium satellite data network. The drifters comprise a corner-radar-reflector type drogue attached to a surface float housing the electronics. The drogue is $\sim$85 cm across and is centered at a depth near 1 m. The surface float is $\sim$20 cm in diameter giving a drag-area-ratio >41 [*Niiler et al.*, 1995]. Microstar drifters follow horizontal motion of water to within 1 to 2 cm s^{-1}, and experience vertical shears of 1 to 2 cm s^{-1} from the top to bottom of the drogue [*Ohlmann et al.*, 2005].

[10] A total of 65 drifters were deployed in groups of three or more during 21 July 2004 to 27 June 2005 (Table 1 and Figure 1). Drifters within each group were deployed with 5–10 m spacing. Drifters were typically deployed between 0800 and 1100 (local time). The experimental plan called for drifters to be retrieved just after 24 h of sampling. Boat availability and boating range limitations ultimately gave rise to drifter tracks that sampled over a broad range of times (Table 1 and Figure 2). Two groups of drifters were often deployed on the same day at different locations to sample multiple flow structures. Attempt was made to choose launch locations that would result in observations of the different flow features that characterize the northern SBC. Roughly half the groups were deployed shoreward of the 100 m isobath where the circulation can differ dramatically from that farther offshore [*Dever et al.*, 1998].

[11] Data processing involved removing positions with poor GPS fixes (amounting to less than 1% of the observations) and linearly interpolating to a regular 10-min time interval. Occasional missing position records were not filled by the interpolation. Velocity at each drifter position was computed using centered differences of positions (first differences at endpoints and data gaps). Water depth from the NOAA National Geophysical Data Center 3 Arc-Second Coastal Relief Model was interpolated to drifter position data.

2.2. Relative Dispersion

[12] Relative dispersion is directly computed from drifter pairs as the time dependent mean square pair separation defined as

$$\boldsymbol{D}^2(t) = \frac{1}{n}\sum_{i \neq j} \left(\boldsymbol{x}_i(t) - \boldsymbol{x}_j(t)\right)^2, \tag{2}$$

where $\boldsymbol{x}_i(t)$ gives the time dependent vector position of drifter i, and the sum is over all possible drifter pairs, n, deployed in a group with initial spacing between 5 and 10 m.

Table 1. Drifter Deployment Characteristics[a]

Deployment Number	Start Date	Sampling Time	Deployment Location	Average Speed	Speed Standard Deviation	Normalized Standard Deviation
1a	7/21/2004	29.1	34.34, 119.61	9.0	5.4	0.60
1b	7/21/2004	44.2	34.33, 119.84	29.6	11.9	0.40
2a	7/26/2004	33.1	34.34, 119.61	26.2	12.3	0.47
2b	7/26/2004	45.1	34.28, 119.78	14.3	4.7	0.33
3a	8/16/2004	38.6	34.34, 119.61	12.7	7.4	0.58
3b	8/16/2004	33.9	34.28, 119.78	22.9	13.0	0.57
4a	10/26/2004	5.2	34.39, 119.83	41.4	12.3	0.30
4b	10/27/2004	60.0	34.33, 119.85	32.7	14.8	0.45
5	11/17/2004	23.6	34.30, 119.93	19.9	6.2	0.31
6	12/9/2004	23.6	34.33, 119.82	39.4	8.2	0.21
7	1/31/2005	45.6	34.23, 119.86	15.0	6.7	0.44
8	2/24/2005	6.4	34.31, 119.82	60.4	6.7	0.11
9a	4/4/2005	25.2	34.32, 119.70	25.3	10.7	0.42
9b	4/4/2005	24.9	34.32, 119.68	24.4	9.8	0.40
10a	4/25/2005	22.3	34.33, 119.70	23.3	14.2	0.61
10b	4/25/2005	29.0	34.32, 119.68	24.4	11.5	0.47
11a	5/23/2005	22.3	34.32, 119.65	21.7	9.7	0.45
11b	5/23/2005	26.5	34.31, 119.63	17.7	9.5	0.53
12a	6/27/2005	29.3	34.31, 119.65	20.1	10.4	0.52
12b	6/27/2005	29.0	34.31, 119.64	22.0	8.0	0.36

[a]Deployment number referenced in text is given in column 1. Deployment date, length of deployment in hours, deployment location, mean velocity in cm s^{-1}, velocity standard deviation in cm s^{-1}, and normalized standard deviation are given in columns 2 through 7, respectively. Velocity statistics are computed from all data collected with all drifters in a cluster. Clusters are defined as the set of drifters that begin sampling within a circle having 50 m diameter. All clusters are triplets except for 4a (pentad), 4b (quadruplet), and 5 (pentad).

Each deployed drifter triplet yields three pairs that are treated independently in the calculation of $\boldsymbol{D}^2(t)$. Independence is assumed to maximize the number of drifter pairs used in computing statistics. Mean time dependent relative dispersion quantities computed separately for the eastward and northward directions are not statistically distinct given the sampling error. The observed mean relative dispersion is thus treated as isotropic, presented as a scalar magnitude, and subsequently indicated as D^2. The mean relative dispersion magnitude for drifters at their initial positions (equation (2) with $t = 0$) is subsequently indicated as D_0^2. Separation distance between drifters i and j is subsequently indicated as D_{ij}, and mean separation distance computed over all available drifter pairs is subsequently indicated as D.

2.3. Mean Square Relative Velocity

[13] The separation velocity of particle pairs undergoing relative dispersion can accelerate as particle separation distance increases. This dependence is explored with the square relative velocity vector between drifters i and j, $\boldsymbol{\delta v}_{ij}^2(t)$

$$\boldsymbol{\delta v}_{ij}{}^2(t) = \left(\frac{d\boldsymbol{D}_{ij}}{dt}(t)\right)^2, \tag{3}$$

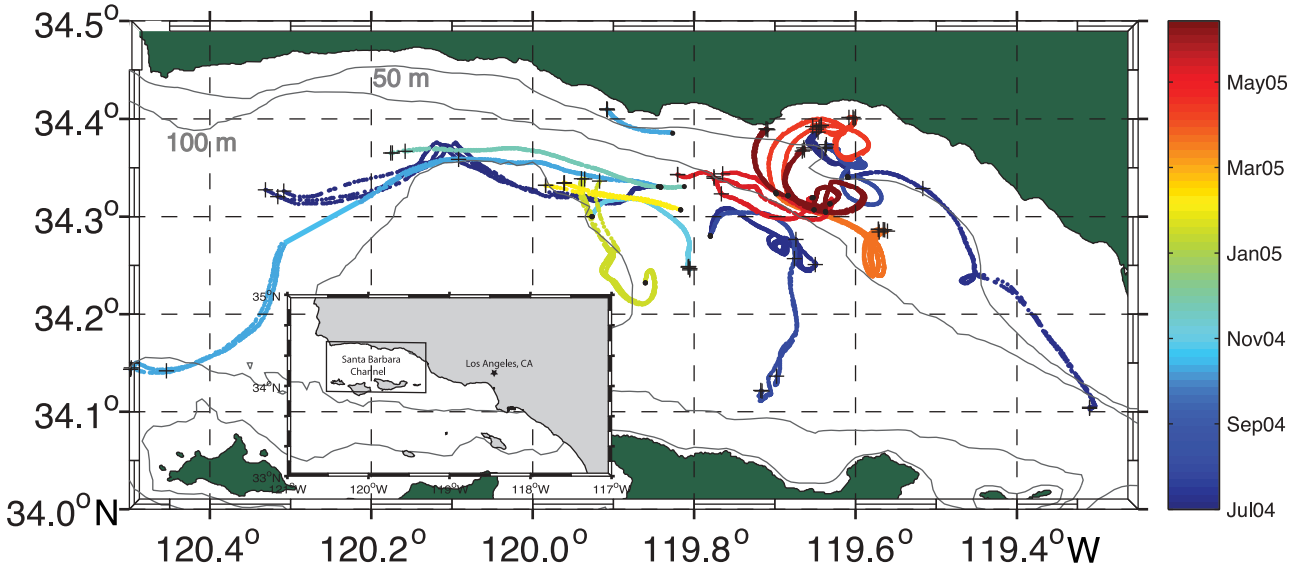

Figure 1. All 65 drifter tracks used in this study (see Table 1) colored by sampling time. Drifter launch positions are shown as black dots and final positions are shown as black crosses. The 50 m, 100 m, and 500 m bathymetry contours are shown in gray. Inset map shows location of the study region within Southern California.

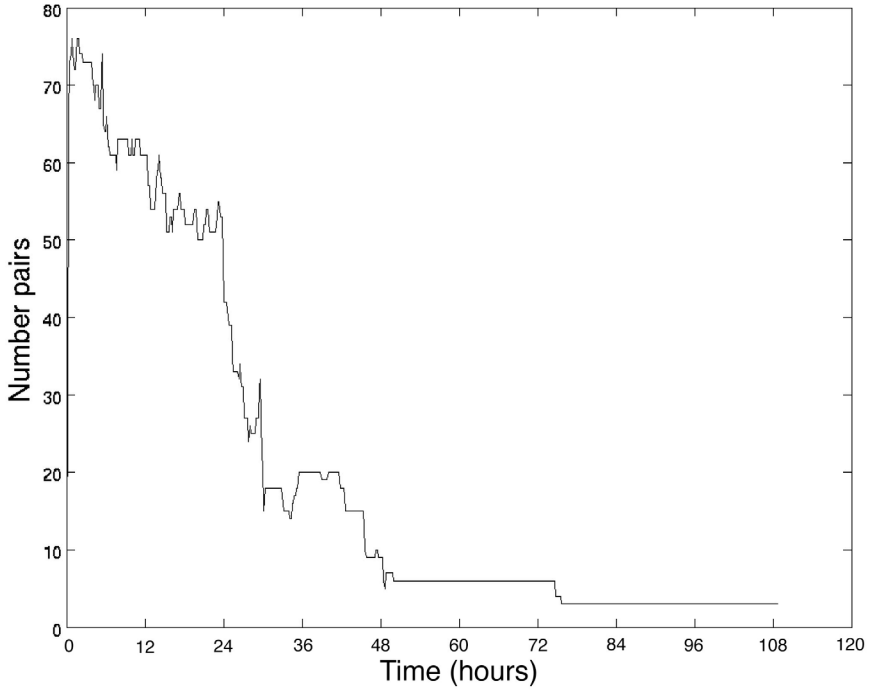

Figure 2. Number of available drifter pairs as a function of time since launch. Small fluctuations in the curve result from occasional missing observations. The experimental plan called for drifter recovery after 24 h.

computed here with all possible drifter pairs, and binned by pair separation distance [e.g., *LaCasce and Bower*, 2000; *Lacorata et al.*, 2004]. Formally $\boldsymbol{\delta v}_{ij}^2(t)$ depends on the vector positions of drifter pairs and is thus a vector quantity. Following the isotropy in D^2 it is treated as having equal components and presented as a scalar magnitude, subsequently indicated as δv^2. Seventeen length bins are defined extending from 7.1 m to 2.6 km, with end points $r_n = r_0(\sqrt{2})^n$; where r_0 = 5 m and n = 1, 2,…,18. δv^2 is determined as a function of length scale by computing the mean of all values within each spatial bin.

2.4. Lagrangian Decorrelation Time

[14] The Lagrangian decorrelation time vector ($\boldsymbol{T}_L$), a time scale over which Lagrangian velocity remains correlated with itself, is defined as the time integral of a Lagrangian velocity autocorrelation function $\boldsymbol{R}_L(\tau)$ [e.g., *Poulain and Niiler*, 1989]

$$\boldsymbol{T}_L = \int_0^T \boldsymbol{R}_L(\tau)\, d\tau. \tag{4}$$

The autocorrelation, $\boldsymbol{R}_{L,i}(\tau)$, is computed for each drifter trajectory i following:

$$\boldsymbol{R}_{L,i}(\tau) = \frac{1}{T}\,\frac{\int_0^T (\boldsymbol{u}_i'(t)\boldsymbol{u}_i'(t+\tau))dt}{\left\langle \boldsymbol{u}_i'^2 \right\rangle_L}, \tag{5}$$

where velocity residual values, $\boldsymbol{u}_i'$, are obtained by removing the mean trajectory velocity from each velocity record for that trajectory, and $\langle\rangle_L$ is the Lagrangian average [e.g., *Poulain and Niiler*, 1989]. $\boldsymbol{R}_L(\tau)$ is then computed as the mean of all $\boldsymbol{R}_{L,i}(\tau)$ values at each time lag τ.

[15] Owing to low frequency motions, $\boldsymbol{T}_L$ can be time dependent and may not asymptote to a well-defined limit. $\boldsymbol{R}_L(\tau)$ is often oscillatory with negative lobes encompassing large areas. These characteristics complicate determination of the interval (T) over which $\boldsymbol{R}_L(\tau)$ is integrated to obtain $\boldsymbol{T}_L$. Integration over a selected time can be inaccurate because errors in $\boldsymbol{R}_L(\tau)$ increase in time [e.g., *Davis*, 1991]. Thus, a common choice, followed here, is integration to the time of the first $\boldsymbol{R}_L(\tau)$ zero crossing [*Swenson and Niiler*, 1996]. As this neglects inclusion of $\boldsymbol{R}_L(\tau) < 0$, resulting $\boldsymbol{T}_L$ estimates subsequently presented are upper bounds.

2.5. Lagrangian Stochastic Modeling

[16] The change in position of particle i, or $d\boldsymbol{x}_i$ over time interval dt, can be modeled following:

$$d\boldsymbol{x}_i = (\boldsymbol{U}_i + \boldsymbol{u}_i)dt, \tag{6}$$

where position and velocity variables are vector quantities, and both velocity terms are time dependent. For particle i, the time dependent change in the stochastic, eddy, or subgrid scale velocity component, indicated $d\boldsymbol{u}_i$, is defined as

$$d\boldsymbol{u}_i = (-\boldsymbol{u}_i\, dt/\boldsymbol{T}_L) + \sqrt{2\boldsymbol{\sigma}_{\boldsymbol{u}}^2/\boldsymbol{T}_L}\; RN, \tag{7}$$

where $\boldsymbol{u}_i$ is the stochastic velocity at time t, dt is the integration time increment, $\boldsymbol{T}_L$ is the Lagrangian decorrelation time vector, $\boldsymbol{\sigma}_{\boldsymbol{u}}$ is the velocity scale vector for the random increment, and RN is a random increment from a normal distribution with zero mean and second order moment $\langle RN*RN\rangle = dt$ (angle brackets represent a mean). Following

the isotropy previous noted, $\boldsymbol{\sigma_u}$ is treated as having has equal components and presented as a scalar magnitude, subsequently indicated as σ_u.

[17] Detailed discussions of the formulation, based on the Langevin equation, are presented in *Sawford* [1985], *Griffa* [1996], and *Berloff and McWilliams* [2002]. Initially, at $\boldsymbol{x}_i(t = 0)$, $\boldsymbol{u}_i = 0$ so $d\boldsymbol{u}_i$ is determined solely from the second term on the right hand side (equation (7)). Implementation of the model requires $dt < \boldsymbol{T}_L$ so that $|-\boldsymbol{u}_i\, dt / \boldsymbol{T}_L| < |\boldsymbol{u}_i|$.

[18] $\boldsymbol{U}$ values used to model trajectories are hourly averaged surface current vectors on a regular 2 × 2 km grid. Eulerian $\boldsymbol{U}$ values derive from HF radar observation with up to five SeaSondes (manufactured by CODAR Ocean Sensors, Los Altos, CA) operating in the 12 to 14 MHz range. HF radar observations in this frequency range give surface currents that are depth integrated over roughly the top 1 m of the ocean [*Stewart and Joy*, 1974]. Each SeaSonde is configured to record hourly average radial velocities in concentric sectors that are 1.5 km in range and 5° in bearing. Spatially averaged eastward and northward velocity components are computed each hour on a 2 km square grid from all radial data within 3 km of a grid-cell center, using the least squares method of *Lipa and Barrick* [1983].

[19] Intermittent gaps of 1–2 h in $\boldsymbol{U}$, characteristic of HF radar observations, are filled by linear interpolation using decomposed empirical orthogonal functions (EOFs) [*Emery and Thomson*, 1998]. Missing values are computed as the mean plus the sum of the first seven EOF modes as described by *Emery et al.* [2006]. EOF gap filling allows LSM trajectories to be computed for the duration of corresponding observed trajectories in all but one case when a several-hour gap occurred. More detailed descriptions of the SBC HF radar SeaSondes, and associated surface current observations are given in *Emery et al.* [2004] and *Ohlmann et al.* [2007].

3. Results

3.1. Lagrangian Flow Descriptions

[20] Drifter groups 1a and 1b were launched on 21 July 2004 in water depths near 50 and 300 m, respectively (Table 1 and Figure 1). Group 1a drifters moved mostly northward (onshore) with a mean speed of 9 cm s^{-1} (Table 1) Group 1b drifters moved westward (up-coast) with a mean speed of 30 cm s^{-1}. The two drifter groups, initially separated by ∼18 km, show remarkably distinct circulation characteristics, with more energetic flow offshore.

[21] Drifter groups 2a and 2b were launched on 26 July 2004 in roughly the same locations as groups 1a and 1b, but moved southeastward mostly along bathymetry (Figure 1). In contrast to groups 1a and 1b, group 2a has a larger mean speed (26 cm s^{-1}) than group 2b (14 cm s^{-1}) which sampled further offshore. Drifter groups 3a and 3b were launched on 16 August 2004, also at the locations of groups 1a and 1b. Drifter groups 3a and 3b initially showed anti-cyclonic circulation. When they stopped turning, group 3a moved westward along bathymetry, and group 3b moved southward (offshore) almost crossing the entire SBC. The southward movement is in opposition to cross-channel flow associated with a cyclonic gyre often present in the western SBC [*Oey et al.*, 2004].

[22] Drifter groups 5 and 7 launched on 17 November 2004 and 31 January 2005, respectively, also moved anticyclonically (Figure 1). Group 5 drifters initially moved northeastward and later turned southward. Group 7 drifters began with northward motion and, after tight rotation, ended with northwestward motion. Separation between drifters that comprise group 7a was the largest observed. Drifter groups 4b, 6, and 8 were deployed near the 300 m isobath on 16 August 2004, 9 December 2004, and 24 February 2005, respectively, and moved westward along bathymetry with mean speeds >30 cm s^{-1}, among the largest observed (Table 1 and Figure 1). One drifter within group 4b, deployed for >4 days, exited the SBC and became entrained into the main southward flowing branch of the California Current System [*Checkley and Barth*, 2009].

[23] Two interesting flow characteristics emerge when considering trajectories of the entire drifter data set. First, only one of the eight drifter clusters deployed west of 119.80°W moved into the eastern SBC. Second, circulation patterns within a few kilometers of the shoreline varied greatly; showing eddy rotation, along- and cross-isobath advection, and a range of velocity magnitudes. The observations are only partly consistent with previous studies showing a large cyclonic gyre in the western half of the SBC, less energetic and more variable flow in the eastern half of the SBC, and a general decrease in energy near the coast [*Dever et al.*, 1998; *Oey et al.*, 2004]. The discrepancy is not surprising as past studies present mean values computed over much longer time periods than considered here.

3.2. Relative Dispersion

[24] D^2 statistics are initially computed from ∼75 drifter pairs (Figure 2). The number of pairs remains larger than 50 during the first 24 h of sampling, but then drops quickly. Only ∼20 pairs sample at 36 h, and <10 pairs sample at 48 h. D^2 observations can be highly variable. Thus, statistics from limited numbers of pairs during the later times have large uncertainties. Nearly all drifter pairs have correlated velocities during the first two sampling days, thereby reducing the effective number of degrees of freedom relative to samples of uncorrelated motion.

[25] D^2 computed from all available drifter pairs shows two distinct regimes (Figure 3). During an initial period, defined as the first 4.8 h of sampling, D^2 increases approximately exponentially in time with an e-folding time of 0.87 h. During the late period, between 4.8 and 46 h, the D^2 increase is approximately quadratic in time, with amplitude 0.3 $km^2\ day^{-2}$. D^2 growth is consistent during the late period despite a drop in the number of available pairs (Figure 2). However, large error bars during the late period (primarily because the number of available pairs is reduced) admit other curve fits as well. D^2 decreases noticeably after 46 h, reflecting the collapse in number of drifter pairs (<10 pairs). Curve fits are with least squares in all cases.

3.3. Mean Square Relative Velocity

[26] Values of δv^2 computed from all available drifter pairs, range from 0.4 $cm^2\ sec^{-2}$ for the 7.1–10.0 m bin, to 85 $cm^2\ sec^{-2}$ for the 1.8–2.6 km bin, and show a near linear increase with length scale (Figure 4). Thus, on average, drifter pairs are accelerating from one another as their relative velocities grow with separation distance. The influence of

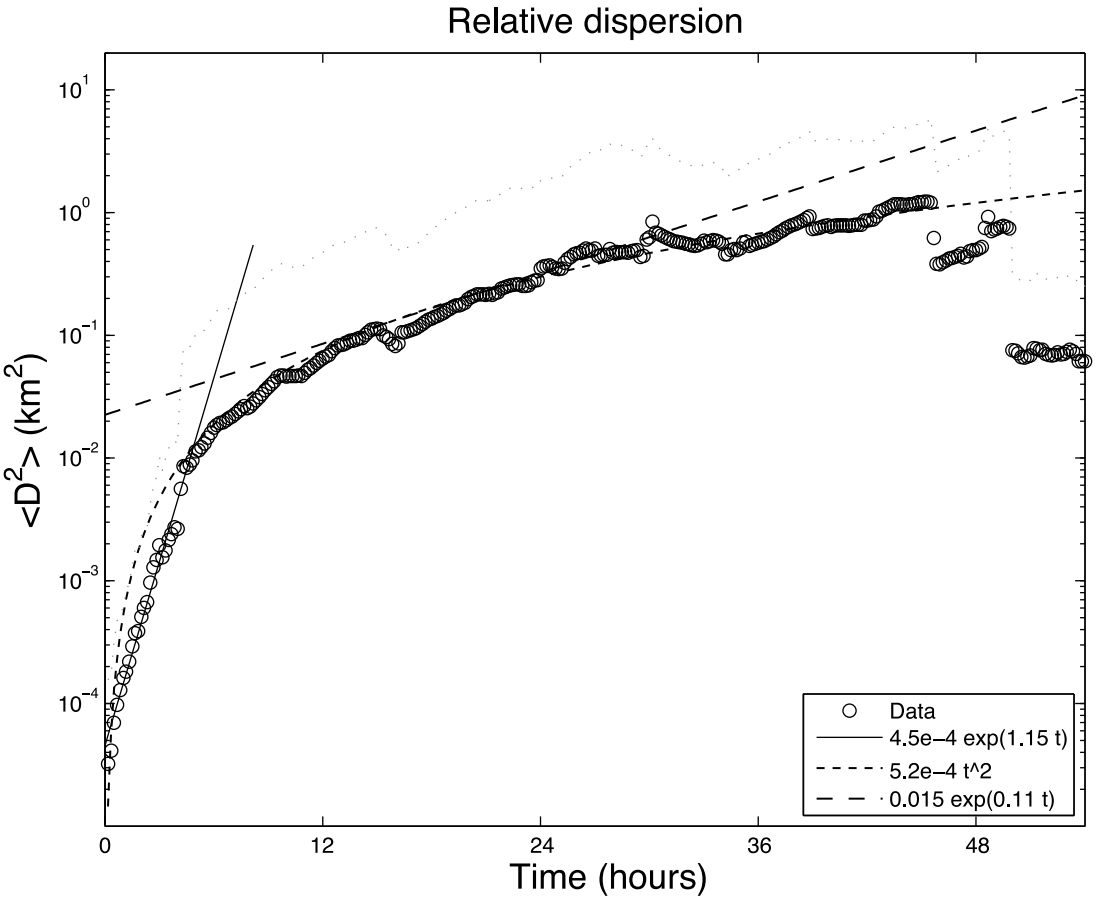

Figure 3. D^2 versus time since launch. Light dotted line indicates the plus one standard deviation curve. A quadratic and two exponential curves fit to the data (dotted, solid and dashed lines) are discussed in the text.

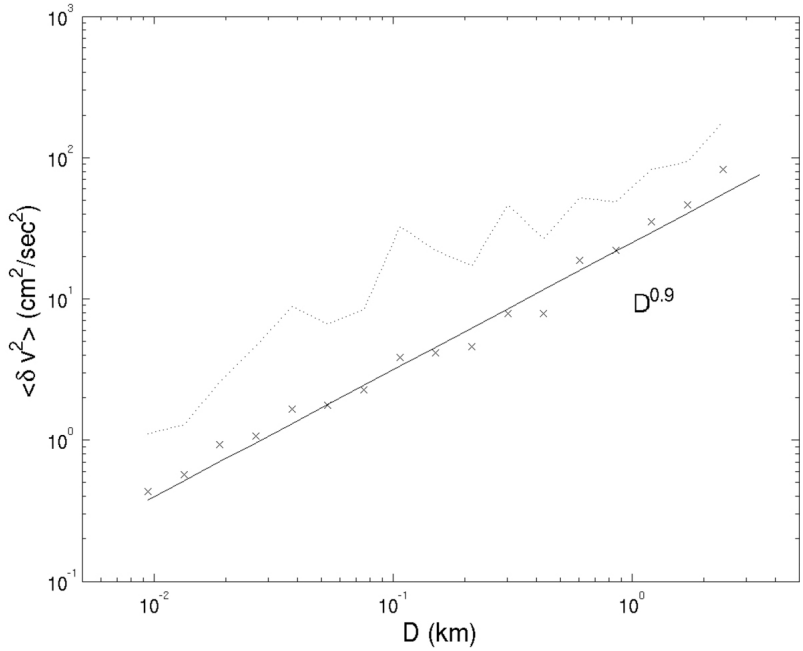

Figure 4. Mean square relative velocity as a function of pair separation distance. The dotted curve shows the upper error bound, defined as +1 standard deviation.

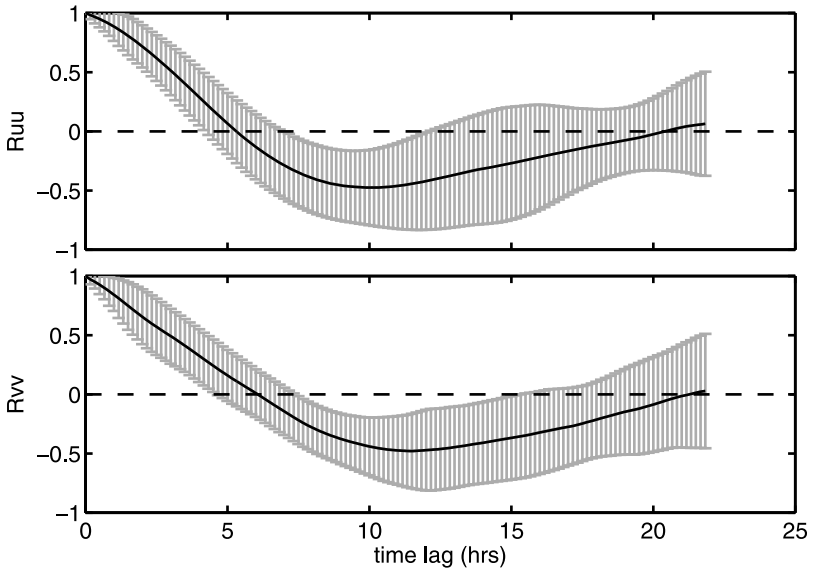

Figure 5. Lagged autocorrelation values computed every 10 min for the u (mostly along shore) and v (mostly across shore) velocity components. Mean values are given in black with gray error bars extending to ±1 standard deviation. Only tracks from drifter deployments longer than 22 h are included in the statistics.

this acceleration on the evolution of a particle cloud is subsequently discussed, and the relationship between δv^2 and length scale in LSM formulation subsequently considered.

3.4. Lagrangian Decorrelation Time

[27] Values of $\boldsymbol{T}_L$ obtained by separately integrating mean autocorrelation curves for the eastward and northward velocity components are both 3.0 h (Figure 5). Results are thus consistent with isotropy in the D^2 analysis. Values are similar to those given by *Ullman et al.* [2006] for the New Jersey shelf, calculated on velocity records of similar length. Values are smaller than previously reported for the SBC (4.8–12 h) [*Dever et al.*, 1998]. However, the *Dever et al.* [1998] estimates are based on drifter observations with significantly less temporal resolution, which may explain the difference.

3.5. Lagrangian Stochastic Modeling

[28] The observed dispersion is now compared with that produced by a LSM. The idea is to simulate the evolution of a cloud of particles originating at the same points as the drifters, and investigate its relative dispersion. The extent to which observed trajectories fall within the modeled cloud is also addressed. The single particle LSM (equation (7)) is used with a modified *RN* term (second term on right side) to account for the observed dependence of δv^2 on D (section 3.3; Figure 4). As will be shown, this model improves results over the standard form that uses a constant $\boldsymbol{\sigma_u}$ (equation (7)). The focus of the LSM work is to demonstrate that a more general model form with scale-dependent $\boldsymbol{\sigma_u}$, and empirically determined parameters, improves agreement with relative dispersion observations.

[29] As previously noted, values of $\boldsymbol{\sigma_u}$ in the LSM derive from δv^2 (components of $\boldsymbol{\sigma_u}$ are equal to $\sqrt{\delta v^2/2}$), and thus have a length scale dependence (Figure 4). This is a significant departure from the formal LSM definition where $\boldsymbol{\sigma_u}$ is equivalent to a standard deviation in Eulerian velocity observations, and is independent of separation scale. Initially, δv^2 is assumed to scale linearly (Figure 4) over a separation range ≤2 km, the grid scale for $\boldsymbol{U}$ from HF radar. Here, σ_u ranges from 0.7 to 5.1 cm s^{-1} for separation scales of 5 m to 2 km, respectively. These values are slightly different than indicated in section 3.3 and shown in Figure 4. LSM trajectories are computed to 24 h and compared with observed trajectories that sample for 24 h. Thus, drifters that sample for <24 h are not used to compute empirical parameters for the LSM. Excluding the shorter tracks does not qualitatively affect results. Similarly, $\boldsymbol{T}_L$ values computed from drifter tracks that sample for at least 24 h do not differ qualitatively from values computed with all available data.

[30] LSM trajectories that begin at the starting times and locations of drifters that sample for at least 24 h (Table 1) are computed in the following manner. The trajectories evolve following equations (6) and (7) using fourth-order Runge-Kutta integration [*Press et al.*, 2002]. A 10-min time step, corresponding to drifter sampling interval, is incorporated through linear interpolation of hourly $\boldsymbol{U}$ data at each grid point. 50 separate LSM trajectories that emanate from the starting time and location of each real drifter (Table 1) are computed. Triplet deployments thus result in LSM trajectories with a total of 150 pairs for calculating D^2 statistics. Least squares fit parameters to D^2 curves computed with LSM trajectories asymptote when the number of pairs (n in equation (2)) reaches ∼75 (not shown). Thus, D^2 curves are expected to be statistically robust when computed with 150 LSM trajectory pairs. Mean D^2 curves computed from LSM trajectories corresponding to all observed drifters that sample for at least 24 h are subsequently indicated as D^2_{mod} (equation (2)).

[31] Observed group 1b trajectories (Table 1), and corresponding LSM trajectory distributions after 24 h, are illustrated in Figure 6a. For this specific case, surface flows are mostly westward between 10 and 50 cm s^{-1}. The

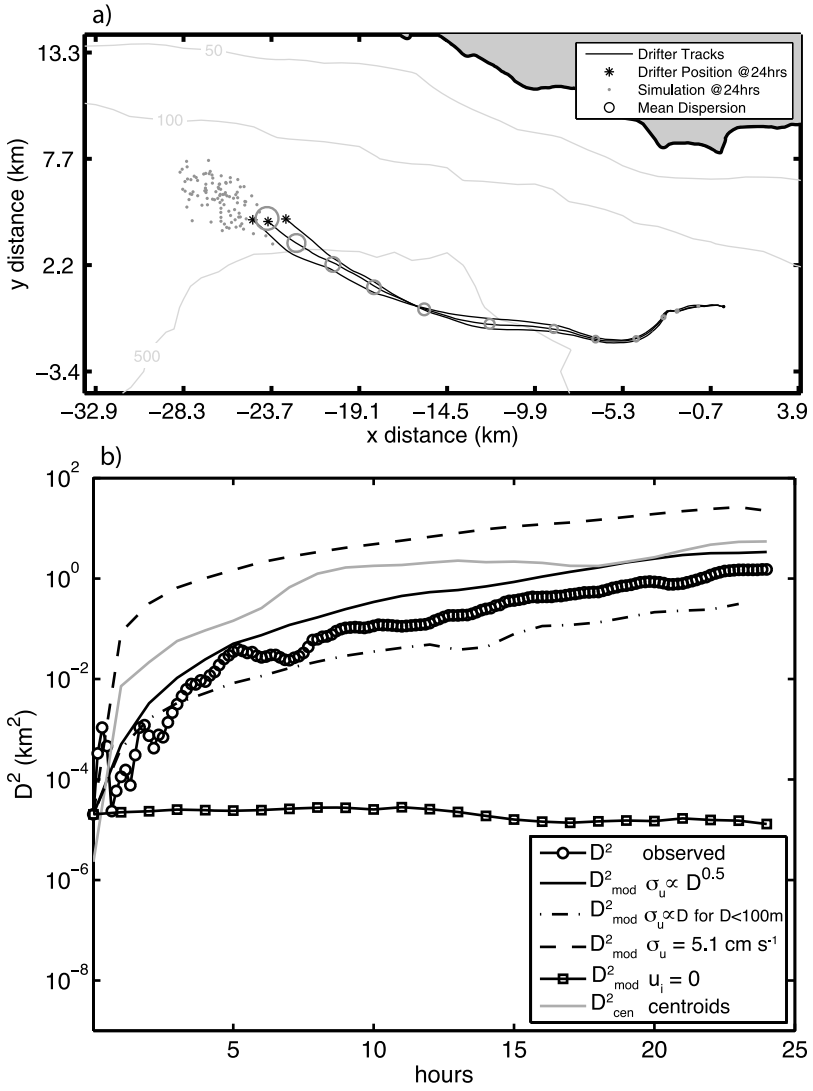

Figure 6. (a) Ending distributions of three observed (asterisk) and 150 corresponding modeled (dots) trajectories after 24 h. Trajectories begin at the origin on 21 July 2004 and are computed from the LSM formulation with $\sigma_u = \delta v$ where $\delta v \propto D^{0.5}$. The entire tracks of observations are shown. Gray circles every 2 h are drawn with radius equal to the square root of the ensemble average D^2 observed, shown in Figure 7. (b) Dispersion from observations on 21 July 2004 shown in Figure 6a, and from corresponding modeled trajectories for that day considering the various LSM formulations presented in section 4. D^2_{mod} is computed with: $\sigma_u = \delta v$ where $\delta v \propto D^{0.5}$ (solid line), $\sigma_u = \delta v$ where $\delta v \propto D^{0.5}$ for $D \geq 100$ m and $\delta v \propto D$ for $D < 100$ m (dash-dot line), $\sigma_u = 5.1$ cm s^{-1} (dashed line), and no sub-grid scale energy ($\boldsymbol{u}_i = 0$; solid line with squares). Gray line shows squared separation between observed and modeled cluster centroids (D^2_{cen}).

group 1b observed trajectories beginning at the origin and ending 24 h later at locations marked with asterisk. Fifty LSM trajectories begin at the starting time and location of each drifter, and their distribution after 24 h is shown with gray dots. The distribution of LSM trajectories is slightly northwest of the observed positions, and partly encompasses the observations. The LSM distribution after 24 h shows greater dispersion than observed.

[32] D^2 and D^2_{mod} for drifter group 1b, shown qualitatively in Figure 6a, are quantified in Figure 6b. Drifter group 1b begins with $D^2_0 = 2.0 \times 10^{-5}$ km^2. Since model trajectories begin at the exact times and locations of the observations, $D^2_{0,\mathrm{mod}} \equiv D^2_0$. D^2 then grows to $1.5 \times 10^{\circ}$ km^2 after 24 h. D^2_{mod} grows slightly faster than observed during the first hour, and remains larger thereafter; there is reasonably good agreement with observations after 24 h.

[33] D^2_{mod} computed from trajectories modeled without a stochastic component (following equation (6) with $\boldsymbol{u}_i = 0$) is nearly constant at 1.5×10^{-5} km^2 (Figure 6b). The small initial separation scale (5–10 m) relative to the much larger $\boldsymbol{U}$ grid scale (2 km) prevents D^2_{mod} growth in the absence of a $\boldsymbol{u}_{\mathrm{i}}$ influence. Trajectories modeled without a stochastic sub-grid scale velocity component have a D^2_{mod} value after 24 h that is five orders of magnitude less than observed. D^2_{mod} computed from trajectories modeled with a constant (scale independent) $\boldsymbol{\sigma_u}$ parameter are much larger than

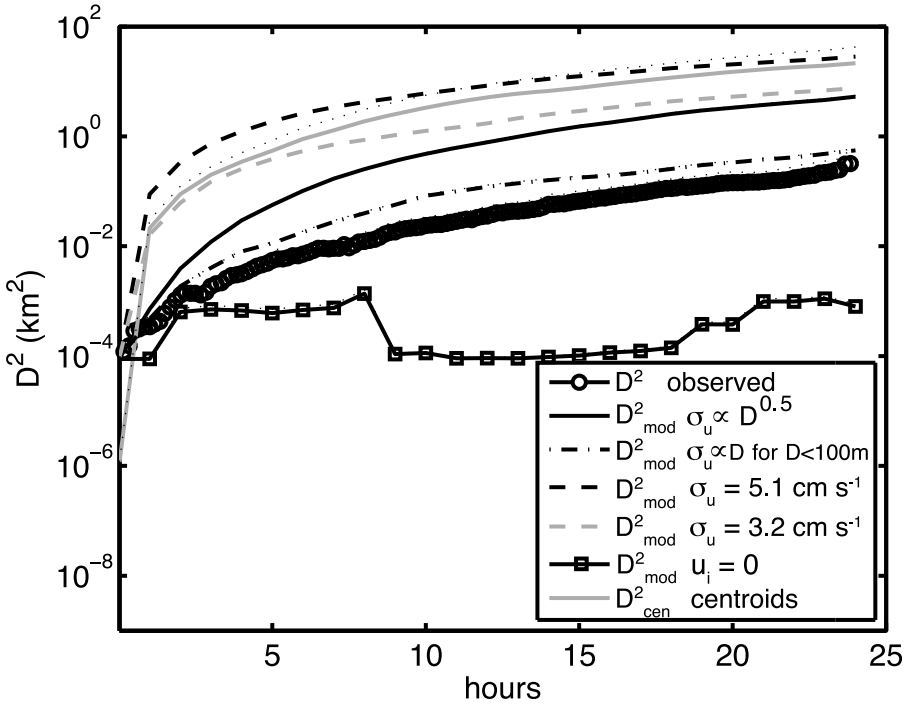

Figure 7. Ensemble average D^2 curves from all sets of observations (circles), and from corresponding sets of modeled trajectories computed with the various LSM formulations presented in section 4. D^2_{mod} is computed with: $\sigma_u = \delta v$ where $\delta v \propto D^{0.5}$ (solid line), $\sigma_u = \delta v$ where $\delta v \propto D^{0.5}$ for $D \geq 100$ m and $\delta v \propto D$ for $D < 100$ m (dash-dot line), $\sigma_u = 5.1$ cm s^{-1} (dashed line), $\sigma_u = 3.2$ cm s^{-1} (dashed gray line), and no sub-grid scale energy ($\boldsymbol{u}_i = 0$; solid line with squares). Solid gray line shows ensemble mean squared separation between observed and modeled cluster centroids (D^2_{cen}).

observed. After 24 h, D^2_{mod} for trajectories from a LSM with $\sigma_u = 5.1$ cm s^{-1}, is 2.2×10^1 km^2, an order of magnitude larger than observed (Figure 6b). At earlier times, between $\sim$1 and 10 h, D^2_{mod} from the LSM with $\sigma_u = 5.1$ cm s^{-1} is two to three orders of magnitude larger than observed. The constant σ_u case is from δv for a separation scale of 2 km, the grid scale for $\boldsymbol{U}$ from HF radar.

[34] Differences in $\boldsymbol{U}$ from HF radar and drifter observations, expected to occur, give rise to time dependent differences between the center of mass of observed and LSM trajectories (hereafter "centroids"). Initially, by definition, centroids of observed and LSM drifter groups are co-located. The centroid difference (D^2_{cen}; expressed as distance squared for consistency) after one hour is 7.2×10^{-3} km^2, and grows to 5.5 km^2 after 24 h (Figure 6b). Good agreement between LSM and observed trajectories occurs when D^2, D^2_{mod}, and D^2_{cen} are all the same order of magnitude, the case for this specific example at times >13 h (Figure 6b).

[35] The separation quantities presented above for drifter group1b (Figure 6a) are computed for the 13 drifter deployments that sampled for at least 24 h (Table 1), and ensemble mean quantities are computed (Figure 7). D^2 grows to 3.2×10^{-1} km^2 after 24 h, consistent with D^2 growth considering the entire data set (2.8×10^{-1} km^2; Figure 3). D^2_{mod} computed from LSM trajectories with $\boldsymbol{u}_i = 0$ is 8.9×10^{-3} km^2 after 24 h, two orders of magnitude less than observed (Figure 7). D^2_{mod} from LSM trajectories with $\sigma_u = 5.1$ cm s^{-1} grows to 2.8×10^1 km^2 after 24 h, two orders of magnitude greater than observed. The introduction of length scale dependency in σ_u (i.e., $\sigma_u = \delta v$) gives $D^2_{mod} = 5.6 \times 10^{\circ}$ km^2 after 24 h, an order of magnitude greater than observed. The cloud model gives the best agreement with D^2 observations by an order of magnitude.

[36] Despite empirical LSM parameters from the observations with which modeled trajectories are compared, the best D^2_{mod} curve, that from the cloud model trajectories ($\sigma_u = \delta v$), is an order of magnitude larger than observed (Figure 7). The cloud model assumes σ_u scales with cloud radius at all times (i.e., $(dD/dt)^2 \propto D$); it is straightforward to show that such a dependence implies D^2 should increase as t^4. This explains why the model initially overestimates the much slower exponential growth observed.

[37] To simulate exponential growth during the initial regime, the δv^2 relationship (Figure 4) is altered so that $\sqrt{\delta v^2} \propto D$ when $D < 100$ m. D^2_{mod} from trajectories computed with this rescaled grows only slightly faster than observed (Figure 7). After 5 h, when a length scale of 100 m is reached, the difference between D^2 and D^2_{mod} is less than an order of magnitude. For length scales beyond 100 m, both D^2 and D^2_{mod} give quadratic growth. After 24 h, $D^2_{mod} = 5.5 \times 10^{-1}$ km^2, the same order of magnitude as observed, and at least an order of magnitude closer to observations compared with the other LSM formulations considered.

4. Discussion

4.1. Relative Dispersion Curve Shape

[38] Relative dispersion in ocean flows has been previously studied with observations from surface drifters and

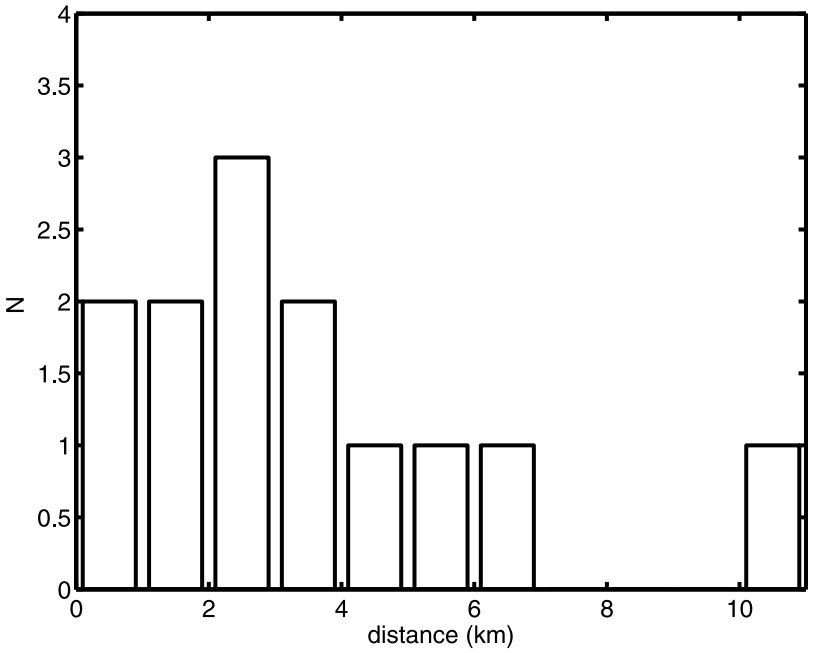

Figure 8. Histogram of x and y distances (distributions are similar for each component) between centroids from observed and modeled drifter clusters after 24 h.

subsurface floats. A number of these studies show exponential growth in relative dispersion below the Rossby deformation radius [*LaCasce and Ohlmann*, 2003; *Ollitrault et al.*, 2005; *Koszalka et al.*, 2009; *Haza et al.*, 2010]. In most of these studies, the smallest separation distance sampled is approximately 1 km. An exception is the *Haza et al.* [2010] study, where use of GPS-tracked drifters (as in this study) allows for initial separations of approximately 100 m. The *Haza et al.* [2010] study shows exponential D^2 growth for separation up to ~1 km, a scale comparable to the deformation radius for the Gulf of La Spezia, their study region.

[39] Exponential growth characterizes *non-local* dispersion, where pair separation is influenced by flow structures larger than the pair separation distance [*Bennett*, 1984]. For non-local dispersion, the energy-wave number spectrum has a slope of k^{-3} or steeper, where k is wave number. Thus, the aforementioned relative dispersion studies suggest steep kinetic energy spectra at sub-deformation scales.

[40] Initial separations in this study are generally between 5 and 10 m, an order of magnitude smaller than previously considered. Exponential growth is observed, but only over separation scales from ~10 to 100 m. The upper limit (100 m) is substantially smaller than the deformation radius for the SBC, expected to be near 20 km [*Auad et al.*, 1998; *Oey et al.*, 2001]. The initial exponential growth observed may suggest drifter pairs are "adjusting" to the advective regime [e.g., *Babiano et al.*, 1990]. That is, pairs are experiencing a transient state where they lose memory of their initial separations. At scales above 100 m dispersion growth is nearly quadratic in time, typical for a shear flow [e.g., *LaCasce*, 2008].

[41] Dispersion curve shapes presented here may not be definitive, as error bars on D^2 observations are large. It is possible to fit a *second* exponential, with an e-folding time of 9 h, within the error bars (Figure 3). This time scale is comparable to that found by *Koszalka et al.* [2009] for surface drifters in the Nordic Seas. Agreement in time scale suggests an exponential fit for separations >100 m is indeed plausible. The observed D^2 veers from quadratic and (*second*) exponential growth after roughly 30 and 46 h, respectively. The departure from exponential growth after 46 h likely results from the number of observed drifter pairs falling quickly to <10 pairs (Figure 2). Observed pair separation distributions are consistent with the expected distributions for exponential growth (not shown) [e.g., *Lundgren*, 1981; *LaCasce*, 2010]. Thus, based on curve fits and pair separation distributions, observed D^2 growth at scales >100 m may be exponential.

[42] The observed relationship between δv^2 and D (Figure 4) raises an objection to exponential D^2 growth at all scales. For *non-local* dispersion that is characterized by exponential growth in D^2, δv^2 dependence should be on D^2 [e.g., *LaCasce*, 2010]. However, observations show δv^2 is closely proportional to D (Figure 4). Given the uncertainty in dispersion curve shape (Figure 3), and the consistent near-linear dependence of the δv^2 diagnostic over the range of scales sampled (Figure 4), the choice was made to focus this work on the role of δv^2 in the formulation of an improved LSM.

4.2. Trajectory Model Evaluation

[43] The standard LSM formulation with constant σ_u (5.1 cm s^{-1}) overestimates D^2 by nearly two orders of magnitude compared with observations (Figure 7). For this model configuration, σ_u comes from δv^2 for the minimum length scale resolved by $\boldsymbol{U}$ (section 3.5). To explore a model configuration with constant σ_u value that is empirically

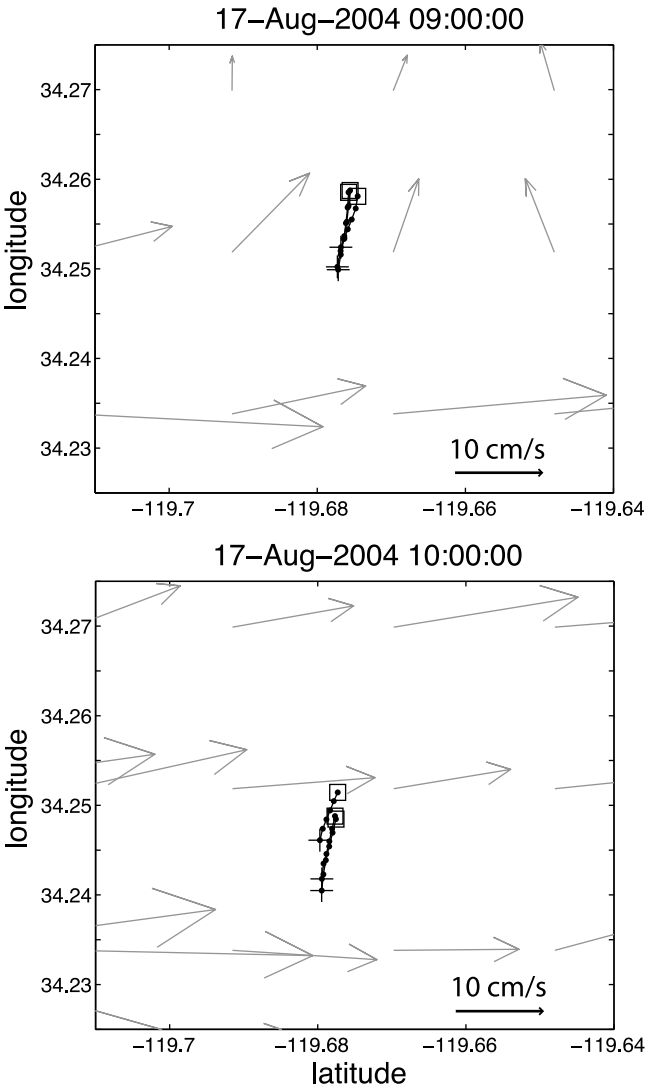

Figure 9. Hourly average HF radar velocity vectors and corresponding drifter position observations during two successive hours. Boxes indicate the starting positions of drifter tracks at the beginning of the hour over which HF radar values are averaged, dots are the drifter positions every 10 min, and plus signs are the ending positions after the hour. Drifter velocities are southward near 20 cm/s.

based and <5.1 cm s^{-1}, σ_u is set equal to 3.2 cm s^{-1}. This value comes from δv^2 computed as the mean of all drifter observations being considered (equation (3); as described in section 2.3 without binning). Decreasing σ_u reduces D^2_{mod} growth, and improves agreement with observations. However, the model configuration yields D^2_{mod} values that still grow faster than observed, and generally exceed observed values by more than an order of magnitude (Figure 7; dashed gray line).

[44] Enforcing the observed scale dependence in σ_u gives D^2_{mod} that agrees better with observations over all times (Figure 7), as initial D^2_{mod} growth is reduced while still permitting larger D^2_{mod} values at later times. The various LSM model configurations (Figure 7) also demonstrate the importance of early time behavior on D^2 values at later times. The approach of incorporating σ_u scale dependency in a LSM is similar to that for stochastic relative dispersion models [e.g., *Sawford*, 2001], as cloud dispersion is closely related to relative dispersion.

[45] Despite data – model agreement in D^2 with the LSM using rescaled δv^2, observed drifter clusters do not, on average, lie within the distribution of LSM trajectories at any time during the 24-h integrations. D^2_{cen} is larger than D^2_{mod} at the first time step, and remains larger throughout the 24-h period considered (Figure 7). The distribution of LSM trajectory positions after 24 h mostly encompasses the observed positions in only 4 of the 13 cases considered. In general, this result is similar to that of *Ullman et al.* [2006] who state LSM trajectories are only an improvement over persistence ("persistence" refers to the assumption that particles persist at their last known location). That is, on average, the ending position of LSM trajectories is closer to the ending position of the observed trajectories than the starting position of the observed trajectories.

[46] The distribution of D_{cen} after 24 h shows instances of both good (≤2 km separation) and poor (>10 km separation) data – model trajectory agreement (Figure 8). Separation of 10 km after 24 h corresponds to a mean velocity difference of ∼11 cm s^{-1} during the period. Coincidently measured surface current velocities from drifters and HF radar can, at times, be grossly different. For a single hour on 17 August 2004, HF radar shows mostly northward flows near 10 cm s^{-1} while a drifter cluster travels in nearly the opposite direction with velocity near 20 cm s^{-1} (Figure 9, top). During the subsequent hour, many of the HF radar velocity $\boldsymbol{U}$ vectors change dramatically, showing eastward flow at roughly 20 cm s^{-1} while the drifter cluster continues southward (Figure 9, bottom).

[47] Perfect agreement between drifter and HF radar velocities is not expected because the instruments make different measurements [*Kohut et al.*, 2006; *Ohlmann et al.*, 2007]. It is however interesting that the two measurements have occasional periods of gross disagreement as shown in Figure 9. Root mean square (RMS) differences between velocities from HF radar and in situ observations are known to be near 10 cm s^{-1} [*Chapman and Graber*, 1997]. Part of the difference is from spatial scale and sampling depth of HF radar when compared with in situ measurements. The large discrepancy illustrated in Figure 9 likely extends beyond the difference in measurements alone. Issues such as RF interference, and errors in direction finding that place observations at an incorrect bearing, may cause occasional erroneous HF radar velocities.

[48] Distributions of differences between drifter and HF radar (interpolated to the time and location of drifter observations) velocity components are near Gaussian with mean values <1 cm s^{-1} (Figure 10). RMS differences for the eastward (u) and northward (v) velocity components are 11.1 and 8.7 cm s^{-1}, respectively. The distributions indicate that velocity differences >20 cm s^{-1} can arise. Such occasional extreme velocity differences prevent consistent agreement between ending distributions of observed and HF radar-based LSM trajectories despite the verity of the cloud dispersion model presented here.

[49] The constant σ_u values (5.1 and 3.2 cm s^{-1}) based on observations of δv^2 are significantly smaller than used in

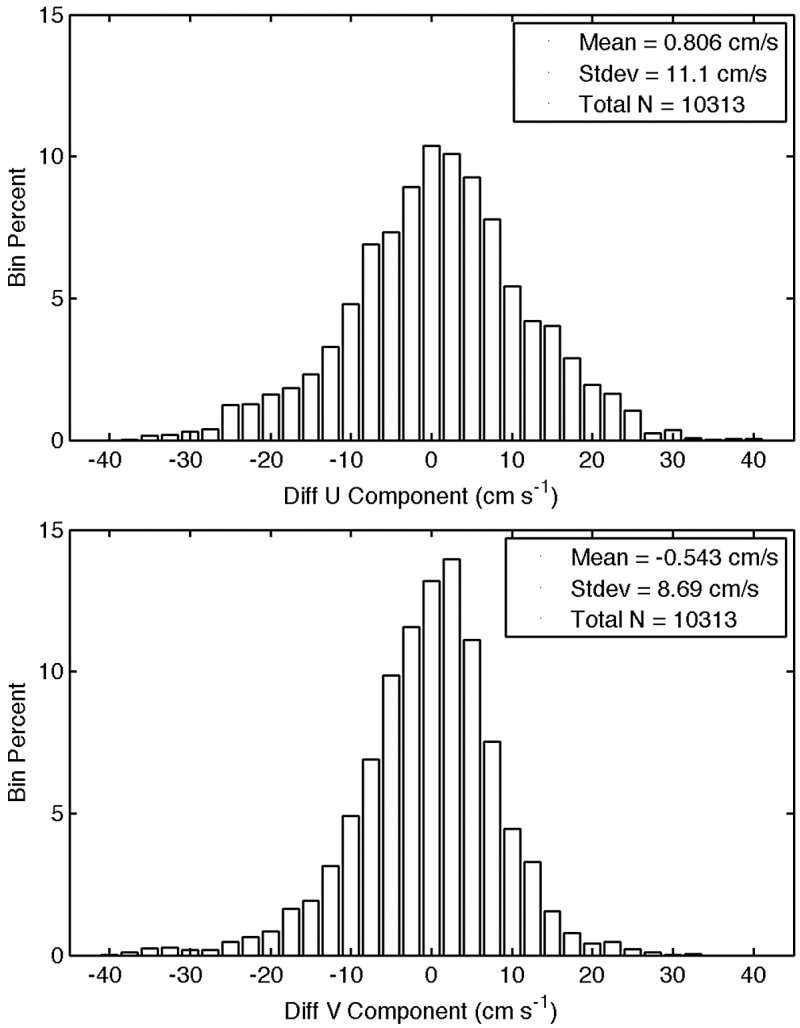

Figure 10. Histogram of differences between drifter and HF radar velocity components. Drifter velocities are computed using a centered difference in 10 min position records (first difference at endpoints and data gaps). HF radar velocities are produced hourly on a 2 × 2 km grid and interpolated to the time and position on which each drifter velocity is centered. The u and v velocity components are oriented mostly in the along shore and cross shore directions, respectively. Histograms are from 10,313 velocity differences.

previous LSM studies. For the New Jersey shelf region, *Ullman et al.* [2006] use σ_u values ranging from 11 to 13 cm s^{-1}, even at the smallest separation scales considered. Use of such a large constant σ_u in a LSM for particles that begin closely spaced (separation <1 km) results in gross overestimation of D^2_{mod} compared with observations. Use of a large and constant σ_u may be desired in some LSM applications. For search-and-rescue, increasing σ_u gives an increased search area that is more apt to encompass the lost object. Such values however are not representative of the true eddy energy that gives rise to the unresolved motions represented through a LSM.

5. Conclusions

[50] Sets of trajectories that begin closely spaced are computed for 24 h from HF radar surface current maps and numerous LSM formulations. Trajectories modeled with no sub-grid scale energy ($\boldsymbol{u}_i = 0$ in equation (6)) exhibit very little dispersion. D^2 after 24 h is more than two orders of magnitude less than observed. Use of a constant σ_u, the typical LSM formulation, gives model dispersion that is roughly two orders of magnitude larger than observed. The constant value selected ($\sigma_u = 5.1$ cm s^{-1}) corresponds to the empirically determined stochastic velocity scale for a separation length scale of 2 km, the minimum length scale resolved with $\boldsymbol{U}$.

[51] A LSM formulation with length scale dependence in the velocity scale for RN ($\boldsymbol{\sigma}_u$ in equation (7)) is proposed for a cloud model where the stochastic velocity component moves trajectories independently about a center of mass. However, D^2_{mod} from LSM trajectories computed with such a cloud model is an order of magnitude larger than from observations. The cloud model with $\delta v \propto D^{1/2}$ gives t^4 dispersion growth during the early period, larger than observed. Rescaling so that $\delta v \propto D$, for $D < 100$ m, gives

D^2_{mod}, that closely matches observations. Realistic LSM formulations require both a more general form, and an observational understanding of the sub-grid scale, or turbulent, processes they must represent. It is unknown if the parameters and scalings presented here are relevant to other coastal regions. D^2 observations in other coastal regions on 5 m to 2 km separation scales are necessary to address this question.

[52] Although D^2 is accurately reproduced, distributions of LSM trajectories after 24 h generally show poor agreement with observations. LSM trajectories encompass measured trajectories for only about 30% of the releases. The generally poor agreement likely results from errors in the use of HF radar-derived Eulerian currents for estimating $\boldsymbol{U}$. Assuming a zero initial condition in the stochastic velocity component may be another problem. After 24 h, average separation between centroids of observed and modeled trajectory sets is ~5 km, corresponding to mean separation velocity of ~6 cm s^{-1} for the period. The centroid separation exceeds 10 km for an individual case. Average centroid D^2 is near two orders of magnitude greater than the observed D^2.

[53] It is well known that drifters and HF radar measure velocity in fundamentally different ways. Primary differences are in horizontal resolution and measurement depth. Given knowledge of surface shear profiles and horizontal variability in the coastal ocean, it is doubtful that very large velocity differences (>~25 cm s^{-1}) during periods when both platforms record modest flow (<~20 cm s^{-1}) can be explained by the discrepancy in measurement techniques alone. Occasional large differences between HF radar and drifter velocities, even during a single hour, prevent consistent agreement between trajectories determined from HF radar observations and in situ observations.

[54] A model formulation that maximizes agreement between observed and modeled trajectories is not a goal of this study. Rather, this work is focused on direct observations of D^2 for the SBC on scales ranging from meters to a kilometer. These separation scales are one to two orders of magnitude smaller than typically observed. D^2 observations show two distinct regimes. Over the first 4.8 h of sampling, and separation scales ranging from ~5 to 100 m, the D^2 increase is roughly exponential with an e-folding time of 0.87 h. Between 4.8 and 46 h, and separation scales ranging from 100 m to 1 km, D^2 growth is roughly quadratic in time. However, relatively few observations give rise to large error bars that admit a number of plausible best fit curves.

[55] The near-linear increase in δv^2 with pair separation distance, extending from 0.3 cm^2 sec^{-2} to 85 cm^2 sec^{-2} over length scales from 7 m to 2.4 km, respectively, is the more robust result. Considering the observed scale dependency in a cloud model does improve the modeled dispersion compared with the traditional LSM formulation that is independent of scale. The study thus informs on eddy kinetic energy and trajectory model parameters for a range of relatively small scales; information that can help guide sub-grid scale parameterizations in numerical models, and relative dispersion representation in trajectory modeling applications.

[56] **Acknowledgments.** Support for this work comes from the National Science Foundation (OCE-0352187). We thank three anonymous reviewers for their constructive comments.

References

Auad, G., M. C. Hendershott, and C. D. Winant (1998), Wind-induced currents and bottom-trapped waves in the Santa Barbara Channel, *J. Phys. Oceanogr.*, *28*, 85–102, doi:10.1175/1520-0485(1998)028<0085:WICABT>2.0.CO;2.

Babiano, A., C. Basdevant, P. Le Roy, and R. Sadourny (1990), Relative dispersion in two-dimensional turbulence, *J. Fluid Mech.*, *214*, 535–557, doi:10.1017/S0022112090000258.

Batchelor, G. K., and A. A. Townsend (1953), Turbulent diffusion, *Surv. Mech.*, *23*, 352–398.

Bennett, A. F. (1984), Relative dispersion: Local and nonlocal dynamics, *J. Atmos. Sci.*, *41*, 1881–1886, doi:10.1175/1520-0469(1984)041<1881:RDLAND>2.0.CO;2.

Berloff, P. S., and J. C. McWilliams (2002), Material transport in oceanic gyres. Part II: Hierarchy of stochastic models, *J. Phys. Oceanogr.*, *32*, 797–830, doi:10.1175/1520-0485(2002)032<0797:MTIOGP>2.0.CO;2.

Chapman, R. D., and H. C. Graber (1997), Validation of HF radar measurements, *Oceanography*, *10*, 76–79.

Checkley, D. M., Jr., and J. A. Barth (2009), Patterns and processes in the California Current System, *Prog. Oceanogr.*, *83*, 49–64, doi:10.1016/j.pocean.2009.07.028.

Davis, R. E. (1987), Modeling eddy transport of passive tracers, *J. Mar. Res.*, *45*, 635–666, doi:10.1357/002224087788326803.

Davis, R. E. (1991), Observing the general circulation with floats, *Deep Sea Res.*, *38*, S531–S571.

Dever, E. P., M. C. Hendershott, and C. D. Winant (1998), Statistical aspects of surface drifter observations of circulation in the Santa Barbara Channel, *J. Geophys. Res.*, *103*, 24,781–24,797, doi:10.1029/98JC02403.

Emery, B. M., L. Washburn, and J. A. Harlan (2004), Evaluating radial current measurements from CODAR high-frequency radars with moored current meters, *J. Atmos. Oceanic Technol.*, *21*, 1259–1271, doi:10.1175/1520-0426(2004)021<1259:ERCMFC>2.0.CO;2.

Emery, B. M., L. Washburn, M. Love, M. M. Nishimoto, and J. C. Ohlmann (2006), Do oil and gas platforms off California reduce recruitment of bocaccio (Sebastes paucispinis) to natural habitat? An analysis based on trajectories derived from high frequency radar, *Fish. Bull.*, *104*, 391–400.

Emery, W. J., and R. E. Thomson (1998), *Data Analysis Methods in Physical Oceanography*, 634 pp., Pergamon, Oxford, U. K.

Griffa, A. (1996), Applications of stochastic particle models to oceanographic problems, in *Stochastic Modeling in Physical Oceanography*, *Prog. Probab. Ser.*, vol. 39, edited by R. J. Adler, P. Müller, and B. Rozovskii, pp. 114–140, Birkhuser, Cambridge, Mass.

Griffa, A., K. Owens, L. Piterbarg, and B. Rozovskii (1995), Estimates of turbulence parameters from Lagrangian data using a stochastic particle model, *J. Mar. Res.*, *53*, 371–401, doi:10.1357/0022240953213151.

Haza, A. C., T. M. Özgökmen, A. Griffa, A. Molcard, P. M. Poulain, and G. Peggion (2010), Transport properties in small scale coastal flows: Relative dispersion from VHF radar measurements in the Gulf of La Spezia, *Ocean Dyn.*, *60*, 861–882, doi:10.1007/s10236-010-0301-7.

Kim, S. Y., et al. (2011), Mapping the U. S. West Coast surface circulation: A multiyear analysis of high-frequency radar observations, *J. Geophys. Res.*, *116*, C03011, doi:10.1029/2010JC006669.

Kohut, J. T., H. J. Roarty, and S. M. Glenn (2006), Characterizing observed environmental variability with HF Doppler radar surface current mappers and acoustic Doppler current profilers: Environmental variability in the coastal ocean, *IEEE J. Oceanic Eng.*, *31*, 876–884, doi:10.1109/JOE.2006.886095.

Koszalka, I., J. H. LaCasce, and K. A. Orvik (2009), Relative dispersion in the Nordic Seas, *J. Mar. Res.*, *67*, 411–433, doi:10.1357/002224009790741102.

LaCasce, J. H. (2008), Statistics from Lagrangian observations, *Prog. Oceanogr.*, *77*, 1–29, doi:10.1016/j.pocean.2008.02.002.

LaCasce, J. H. (2010), Relative displacement PDFs in 2-D turbulence and observations, *J. Mar. Res.*, *68*, 433–457, doi:10.1357/002224010794657155.

LaCasce, J. H., and A. Bower (2000), Relative dispersion in the subsurface North Atlantic, *J. Mar. Res.*, *58*, 863–894, doi:10.1357/002224000763485737.

LaCasce, J. H., and C. Ohlmann (2003), Relative dispersion at the surface of the Gulf of Mexico, *J. Mar. Res.*, *61*, 285–312, doi:10.1357/002224003322201205.

Lacorata, G., E. Aurell, B. Legras, and A. Vulpiani (2004), Evidence for a $\kappa^{-5/3}$ spectrum from the EOLE Lagrangian balloons in the low stratosphere, *J. Atmos. Sci.*, *61*, 2936–2942, doi:10.1175/JAS-3292.1.

Lipa, B. J., and D. E. Barrick (1983), Least-squares methods for the extraction of surface currents from CODAR cross-loop data: Application at ARSLOE, *IEEE J. Oceanic Eng.*, *8*, 226–253, doi:10.1109/JOE.1983.1145578.

Lundgren, T. S. (1981), Turbulent pair dispersion and scalar diffusion, *J. Fluid Mech.*, *111*, 27–57, doi:10.1017/S0022112081002280.

Mitarai, S., D. A. Siegel, J. R. Watson, C. Dong, and J. C. McWilliams (2009), Quantifying connectivity in the coastal ocean, *J. Geophys. Res.*, *114*, C10026, doi:10.1029/2008JC005166.

Niiler, P. P., A. L. Sybrandy, K. Bi, P. M. Poulain, and D. Bitterman (1995), Measurements of the water following capability of holey-sock and TRISTAR drifters, *Deep Sea Res. Part I*, *42*, 1951–1964, doi:10.1016/0967-0637(95)00076-3.

Oey, L.-Y., D.-P. Wang, T. Hayward, C. Winant, and M. Hendershott (2001), "Upwelling" and "cyclonic" regimes of the near-surface circulation in the Santa Barbara Channel, *J. Geophys. Res.*, *106*, 9213–9222, doi:10.1029/1999JC000129.

Oey, L.-Y., C. Winant, E. Dever, W. Johnson, and D.-P. Wang (2004), A model of the near-surface circulation of the Santa Barbara Channel: Comparison with observations and dynamical interpretations, *J. Phys. Oceanogr.*, *34*, 23–43, doi:10.1175/1520-0485(2004)034<0023:AMOTNC>2.0.CO;2.

Ohlmann, J. C., P. F. White, A. L. Sybrandy, and P. P. Niller (2005), GPS-cellular drifter technology for coastal ocean observing systems, *J. Atmos. Oceanic Technol.*, *22*, 1381–1388, doi:10.1175/JTECH1786.1.

Ohlmann, J. C., P. F. White, L. Washburn, E. Terrill, B. Emery, and M. Otero (2007), Interpretation of coastal HF radar-derived surface currents with high-resolution drifter data, *J. Atmos. Oceanic Technol.*, *24*, 666–680, doi:10.1175/JTECH1998.1.

Ollitrault, M., C. Gabillet, and A. Colin de Verdiere (2005), Open ocean regimes of relative dispersion, *J. Fluid Mech.*, *533*, 381–407, doi:10.1017/S0022112005004556.

Paris, C. B., L. M. Cherubin, A. Srinivasan, and R. K. Cowen (2007), Surfing, spinning, or diving from reef to reef: How does it change population connectivity?, *Mar. Ecol. Prog. Ser.*, *347*, 285–300, doi:10.3354/meps06985.

Poulain, P. M., and P. P. Niiler (1989), Statistical analysis of the surface circulation of the California Current System using satellite-tracked drifters, *J. Phys. Oceanogr.*, *19*, 1588–1603, doi:10.1175/1520-0485(1989)019<1588:SAOTSC>2.0.CO;2.

Press, W. H., S. A. Teukolsky, W. T. Vetterling, and B. P. Flannery (2002), *Numerical Recipes in C: The Art of Scientific Computing*, Cambridge Univ. Press, Cambridge, U. K.

Richardson, L. F. (1926), Atmospheric diffusion on a distance–neighbour graph, *Proc. R. Soc. London, Ser. A*, *110*, 709–737, doi:10.1098/rspa.1926.0043.

Sawford, B. L. (1985), Lagrangian statistical simulation of concentration mean and fluctuation fields, *J. Clim. Appl. Meteorol.*, *24*, 1152–1166, doi:10.1175/1520-0450(1985)024<1152:LSSOCM>2.0.CO;2.

Sawford, B. L. (2001), Turbulent relative dispersion, *Annu. Rev. Fluid Mech.*, *33*, 289–317, doi:10.1146/annurev.fluid.33.1.289.

Spaulding, M. L., T. Isaji, P. Hall, and A. A. Allen (2006), A hierarchy of stochastic particle models for search and rescue (SAR): Application to predict surface drifter trajectories using HF radar current forcing, *J. Mar. Environ. Eng.*, *8*, 181–214.

Stewart, R. H., and J. W. Joy (1974), HF radio measurements of ocean surface currents, *Deep Sea Res. Oceanogr. Abstr.*, *21*, 1039–1049.

Swenson, M. S., and P. P. Niiler (1996), Statistical analysis of the surface circulation of the California Current, *J. Geophys. Res.*, *101*, 22,631–22,645, doi:10.1029/96JC02008.

Taylor, G. I. (1922), Diffusion by continuous movements, *Proc. London Math. Soc.*, *s2-20*, 196–212, doi:10.1112/plms/s2-20.1.196.

Ullman, D. S., J. O'Donnell, J. Kohut, T. Fake, and A. Allen (2006), Trajectory prediction using HF radar surface currents: Monte Carlo simulations of prediction uncertainties, *J. Geophys. Res.*, *111*, C12005, doi:10.1029/2006JC003715.

Veneziani, M., A. Griffa, A. M. Reynolds, and A. J. Mariano (2004), Oceanic turbulence and stochastic models from subsurface Lagrangian data for the north-west Atlantic Ocean, *J. Phys. Oceanogr.*, *34*, 1884–1906, doi:10.1175/1520-0485(2004)034<1884:OTASMF>2.0.CO;2.

Wilson, J. D., and B. L. Sawford (1996), Review of Lagrangian stochastic models for trajectories in the turbulent atmosphere, *Boundary Layer Meteorol.*, *78*, 191–210, doi:10.1007/BF00122492.